frontiers in Earth Science

HYPOTHESIS AND THEORY
published: 10 July 2020
doi: 10.3389/feart.2020.00244

Effects of Oceanic Crustal Thickness on Intermediate Depth Seismicity

Lara S. Wagner[1], Mark J. Caddick[2], Abhash Kumar[3], Susan L. Beck[4] and Maureen D. Long[5]*

[1] Department of Terrestrial Magnetism, Carnegie Institution for Science, Washington, DC, United States, [2] Department of Geosciences, Virginia Polytechnic Institute and State University, Blacksburg, VA, United States, [3] Department of Geology and Environmental Science, University of Pittsburgh, Pittsburgh, PA, United States, [4] Department of Geosciences, University of Arizona, Tucson, AZ, United States, [5] Department of Geology and Geophysics, Yale University, New Haven, CT, United States

The occurrence of intermediate depth seismicity (70–300 km) is commonly attributed to the dehydration of hydrous phases within the downgoing oceanic plate. While some water is incorporated into the oceanic crust at formation, a significant amount of water is introduced into the plate immediately before subduction along outer-rise faults. These faults have been shown to extend to depths of over 30 km and can channel water to depths of 20 km or more beneath the seafloor. However, the amount of water introduced into the oceanic mantle lithosphere, and the role of that water in the formation of intermediate depth seismicity, has been the topic of ongoing research. Here we compile evidence from areas where the subducted oceanic crust is likely thicker than the penetration depth of water into the downgoing plate. These regions comprise aseismic plateaus and ridges (hot spot tracks) that can be compared directly to adjacent segments of the oceanic plate where oceanic crust of normal thickness is subducted. Regions with thick oceanic crust show little to no seismicity at intermediate depths, whereas adjacent regions with normal oceanic crust (~6–8 km thick) have significant seismicity at similar depths and distances from the trench. We hypothesize that intermediate depth earthquakes observed in regions with thinner oceanic crust are caused by mantle dehydration reactions that are not possible in regions where the oceanic mantle was never hydrated because the thickness of the oceanic crust exceeded the penetration depth of water into the plate. We compare our observations to phase diagrams of hydrous basalt and hydrated depleted peridotite to determine pressures and temperatures that would be consistent with our observations. These can provide valuable constraints, not only on the degree of hydration and dehydration in the downgoing plate, but also as ground-truth for thermal models of these regions, all of which have complex, three-dimensional, time-variant subduction geometries and thermal histories.

Keywords: flat-slab, seismicity, hydration, intermediate-depth, aseismic-ridges, oceanic crust, oceanic ridges

OPEN ACCESS

Edited by:
Vlad Constantin Manea, National Autonomous University of Mexico, Mexico

Reviewed by:
Fenglin Niu, Rice University, United States
Wasja Bloch, German Research Centre for Geosciences, Helmholtz Centre Potsdam, Germany

****Correspondence:***
Lara S. Wagner
lwagner@carnegiescience.edu

Specialty section:
This article was submitted to Structural Geology and Tectonics, a section of the journal Frontiers in Earth Science

Received: *28 December 2019*
Accepted: *04 June 2020*
Published: *10 July 2020*

Citation:
Wagner LS, Caddick MJ, Kumar A, Beck SL and Long MD (2020) Effects of Oceanic Crustal Thickness on Intermediate Depth Seismicity. Front. Earth Sci. 8:244. doi: 10.3389/feart.2020.00244

INTRODUCTION

Intermediate depth earthquakes (70–300 km depth) occur at pressures and temperatures (P/T) that should produce ductile deformation rather than brittle failure (e.g., Green and Houston, 1995). There has long been significant debate about the role of dehydration reactions in the formation of intermediate depth seismicity. The P/T conditions at which intermediate depth earthquakes occur have repeatedly been shown to be consistent with dehydration phase boundaries for both crustal and mantle lithospheric hydrous compositions (e.g., Kirby, 1995; Kirby et al., 1996; Peacock, 2001; Hacker et al., 2003; Yamasaki and Seno, 2003; Abers et al., 2013). The most commonly cited link between dehydration and intermediate depth seismicity is dehydration embrittlement. As originally conceived, the term "dehydration embrittlement" means the hydraulic fracturing of rock caused by the production of free fluids and resultant overpressure in pore spaces that in turn could overcome the ambient pressure (e.g., Raleigh and Paterson, 1965; Meade and Jeanloz, 1991). However, more recent experimentation has shown that (a) above some pressure, volume change associated with dehydration reactions is likely negative, complicating the overpressure argument (e.g., Dobson et al., 2002; Jung et al., 2004; Gasc et al., 2011), and (b) some experiments on antigorite and other hydrous phases have produced no acoustic emissions (AEs) upon dehydration and/or show evidence solely of stable sliding or distributed deformation, bringing the concept of "dehydration embrittlement" into question (e.g., Chernak and Hirth, 2010; Chernak and Hirth, 2011; Gasc et al., 2011; Proctor and Hirth, 2015; Gasc et al., 2017). One possible contribution from dehydration reactions unrelated to pore pressure is the formation of nanocrystalline reaction products whose small grain size might contribute to vein growth, channel flow, and/or localized weakening (e.g., Incel et al., 2017; Plümper et al., 2017). Other theories have focused more directly on localized weakening due to slip, i.e., thermal run-away/shear heating mechanisms that also incorporate reduced grain size along discrete planes of weakness (e.g., Kelemen and Hirth, 2007; John et al., 2009; Prieto et al., 2013; Poli et al., 2016; Proctor and Hirth, 2016; Ohuchi et al., 2017). Thermal run-away mechanisms may be self-initiating or may serve as a propagation mechanism for events triggered by another mechanism (e.g., Zhan, 2017). A recent theory that matches many of these observations is the "dehydration destabilization stress transfer" mechanism (DDST; Ferrand et al., 2017; Ferrand, 2019). In this model, hydrated peridotite produces AEs at specific conditions that depend on the amount of hydrated material present within the peridotite matrix and the pressure at which the dehydration reaction occurs. Rather than increasing pore pressure to hydraulically fracture the surrounding rock matrix, the dehydration of antigorite (or other hydrous phases) results in an extreme weakening and volume decrease of the dehydrating phase, which in turn transfers ambient stresses onto the enclosing dry peridotite rock matrix. The amount of hydrous phase in the rock has to be sufficient that its dehydration-related weakening will sufficiently load the surrounding matrix to the point of failure, but not so great that the surrounding matrix does not possess sufficient strength to accumulate strain. According to the calculations of Ferrand et al. (2017) at 3.5 GPa, relatively little antigorite (∼5%) is needed to induce seismicity, consistent with small amounts of hydrated material that might be present deep within the mantle lithosphere of subducted slabs.

There has also been increased interest in the relationship between observations of heterogeneities within the oceanic plate as it enters the trench, and seismicity patterns in the subducting slab at intermediate depths (e.g., Shillington et al., 2015). Recent studies looking at the seismic velocity structure of oceanic plates as they approach the trench show that outer-rise faulting consistently results in extensive hydration of the oceanic plate (see Grevemeyer et al., 2018 and references therein). In studies with sufficiently deep resolution, hydration is observed to extend ∼10–12 km below the oceanic Moho (e.g., Ranero et al., 2003). Fromm et al. (2006) used aftershock locations from a M_w 6.7 outer-rise earthquake to show faulting to depths of ∼ 25 km. In rare cases (e.g., Bloch et al., 2018; Cai et al., 2018), evidence exists for even deeper hydration. Recent work by Boneh et al. (2019) shows a correlation between the observed fault offsets on outer-rise faults from bathymetry data and the rate of intermediate depth seismicity observed down-dip, which suggests the extent of hydration in the oceanic plate due to outer rise faulting may control the amount of seismicity that is possible at intermediate depths.

While links between hydration and seismicity are consistent with dehydration embrittlement or related mechanisms, they do not address whether it is the dehydration of the oceanic crust or mantle that is responsible for the generation of intermediate depth earthquakes. Our hypothesis is that regions with thinner oceanic crust produce intermediate depth seismicity due to mantle dehydration reactions, and that slabs with very thick oceanic crust do not produce intermediate depth events because the previously hydrated overthickened crust has already experienced its most important dehydration reactions by this point, and because the mantle below was never hydrated to begin with and therefore cannot produce the dehydration reactions needed to generate seismicity.

Our hypothesis is based on the clearest and simplest observation of this pattern: along the Nazca Ridge in Peru (∼18 km thick oceanic crust) (Hampel et al., 2004; Kumar et al., 2016). We present our hypothesis in the context of this location, and investigate other possible factors such as plate age, evidence for outer rise faulting, oceanic crustal structure, and any available direct evidence for oceanic mantle hydration. We also investigate the plausibility of our hypothesis in terms of the metamorphic reactions and pressure-temperature conditions required for this to be true. We then assess the hypothesis at a number of other locations where overthickened oceanic crust is being subducted, including the Juan Fernandez Ridge in Chile which produces an overabundance of seismicity rather than an absence thereof, the Carnegie Ridge subducting beneath Ecuador, and the Cocos Ridge subducting beneath Costa Rica. We show that while these other situations are often more complicated and less clear, they are each consistent with our hypothesis given existing data. Finally, we suggest a number of regions where additional research could be used for further testing of this hypothesis, and could help

to constrain the relationship between water penetration depth, crustal thickness, and intermediate depth seismicity.

NAZCA RIDGE SEISMICITY PATTERNS WITHIN THE PERUVIAN FLAT SLAB

The Nazca Ridge comprises a 1200 km long, ∼200 km wide seamount chain that extends southwest from the southern Peruvian margin. The crustal structures of the Nazca Ridge and adjacent regions of "typical" Nazca plate are constrained by analyses of a suite of trench perpendicular and trench parallel active source surveys and gravity studies (e.g., Hampel et al., 2004; Krabbenhoeft et al., 2004; Grevemeyer et al., 2018; Contreras-Reyes et al., 2019). These show a ∼100 km wide (trench parallel), 17 km thick crustal root beneath the Nazca Ridge, thinning to ∼6.4 km on either side (**Figure 1**). These crustal thickness results are consistent with earlier surface wave dispersion estimates of ∼18 km (Woods and Okal, 1994). The Nazca Ridge's conjugate on the Pacific Plate, the Tuamotu Ridge, has been used to determine the initial timing of collision of this ridge with the South American continent at ∼15–12 Ma, and to project its current location onto the subducted slab (i.e., Pilger, 1981; Woods and Okal, 1994; Gutscher et al., 1999b; Hampel, 2002; Rosenbaum et al., 2005). The difference in the strike of the Nazca Ridge and the relative convergence direction between the Nazca and South American plates (see **Figure 1**) has resulted in a progressive southward migration of the ridge relative to the overriding continental margin since that time (i.e., Gutscher et al., 1999b; Rosenbaum et al., 2005). This, together with the inferred subduction of the conjugate to the Marquesas Plateau, named the Inca Plateau, are often cited as contributing to the formation of the unusually long (along strike) extent of the Peruvian flat slab (i.e., Gutscher et al., 1999b; Antonijevic et al., 2015). The current location of the Nazca Ridge beneath the South American continent has been assessed using adjacent oceanic magnetic anomalies that allow for an alignment of the projection of the conjugate Tuamotu Plateau both along the Nazca Ridge and to regions of the slab already subducted (Hampel, 2002). Note that this location depends only on observations of magnetic anomalies and does not make assumptions about current or past relative plate motions.

Over the past decade, three broadband seismic deployments (PULSE: Wagner et al., 2010; CAUGHT: Beck et al., 2010; PeruSE, 2013) have collected data in central and southern Peru, providing dense seismic coverage across the projected location of the Nazca Ridge. Tomographic and scattered wave imaging based on these data indicate that, as with many regions with subducted overthickened oceanic crust, the projected location of the subducted Nazca Ridge coincides closely with the shallowest portion of the southern Peruvian flat slab (Antonijevic et al., 2015, 2016; Bishop et al., 2017; Wagner and Okal, 2019).

The hypothesis that thicker oceanic crust could lead to an absence of intermediate depth seismicity was first proposed by Kumar et al. (2016) in their study of intermediate depth seismicity using the PULSE, CAUGHT, and PeruSE networks in Peru. The earthquake locations from recent studies using local data (Kumar et al., 2016; Lim et al., 2018) are roughly consistent with catalog data available from the International Seismological Center for events occurring 1990–2017 (International Seismological Centre, 2019 Reviewed Event Catalog, retrieved October 1, 2019). Notably, there is a distinct gap in seismicity located in the middle of the PULSE array where event locations using these data should be most complete (Hampel, 2002; Kumar et al., 2016). This gap corresponds closely to the projected location of the subducted Nazca Ridge based on the projected location of the Tuamotu Plateau (**Figure 1**). The Tuamotu Plateau, however, is much broader than the unsubducted portions of the Nazca Ridge, highlighting the uncertainties about the geometry of the Nazca Ridge location and crustal thickness at depth. However, we note that the region of the observed seismic gap is well within the contours of the projected Tuamotu Plateau, consistent with our hypothesis, and consistent with previous observations of the correlation between the modern projection of the Tuamotu Plateau and the observed gap in seismicity (e.g., Hampel, 2002).We note, however, that at depths shallower than 60 km (i.e., closer to the trench), there is no gap in seismicity along the projected Nazca Ridge track. The right-hand panel of **Figure 1** (A,A′) shows the locations of intermediate depth earthquakes within 75 km of the roughly ridge-perpendicular cross section extending from (−11.3°S; −76.9°W) to (−16.8°S; −71.1°W). Also shown is the oceanic Moho topography and bathymetry from Contreras-Reyes et al. (2019), showing the wavelength of the overthickened crust associated with the Nazca Ridge, which is similar to the size of the gap in seismicity. The red line plotted beneath the seismicity profile indicates the top of the subducted slab as determined by Antonijevic et al. (2015) and Wagner and Okal (2019). Unfortunately, while receiver function studies such as Bishop et al. (2017) are able to identify seismic conversions from the oceanic Moho in some places, the errors in absolute depth for both the receiver functions and the earthquake locations make a determination of whether these events are occurring in the slab crust or mantle impossible.

While it is not currently possible to know the detailed structure of the already subducted Nazca plate collocated with these observed seismicity patterns, it is instructive to look directly offshore at the structure of the Nazca Ridge and adjacent areas that are about to be subducted to infer some constraints on possible structures that could be influencing intermediate depth seismicity. The age of the Nazca plate at the Peruvian margin along and adjacent to the Nazca Ridge varies only slightly from 43 to 46 Ma, except south of the Nazca Fracture Zone (south of our study area) where ages increase to ∼52 Ma (Mueller et al., 2008). This is significant because the age of the plate strongly affects the temperature, and therefore the potential locations of dehydration reactions. In this case, not only is the overall range in ages small, intermediate depth seismicity is located on either side of the gap at the Nazca Ridge, while plate age increases monotonically from north to south. It is therefore unlikely that plate age or slab temperature are responsible for the observed seismicity patterns.

Another possible explanation for this pattern is that the thick crust of the subducting Nazca Ridge does not form as many outer-rise faults as the adjacent thinner oceanic crust, and is therefore

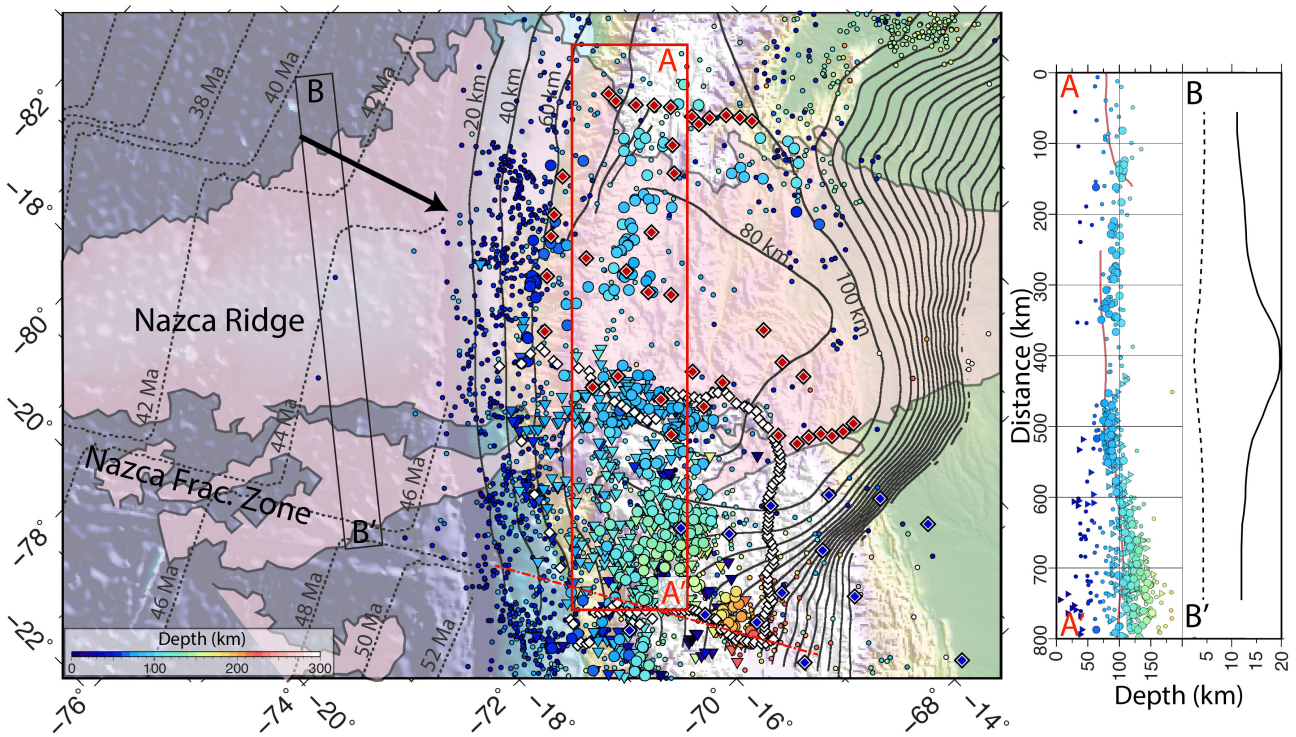

FIGURE 1 | Nazca Ridge subduction and earthquake distribution. **Left:** Map showing seismicity from the Reviewed International Seismological Center's earthquake catalog (1990–2017) – small circles. Large circles are hypocenters from Kumar et al. (2016), and inverted triangles are hypocenters from Lim et al. (2018). Offshore dashed lines show oceanic plate age contours from Mueller et al. (2008). Bold arrow shows convergence direction from DeMets et al. (2010). Pink shaded region shows the outline of the projected conjugate Tuamotu Ridge from Hampel (2002). Red diamonds, blue diamonds, and white diamonds show seismic station locations for the PULSE, CAUGHT, and PERUSE experiments, respectively. Dash-dot red line shows inland projected location of Nazca Fracture Zone. Solid black lines show slab contours from Wagner and Okal (2019). Red rectangular box shows area over which events were projected onto cross section to the right. Black rectangular box shows region over which oceanic Moho topography was compiled by Contreras-Reyes et al., 2019. **Right:** Cross-section across the projected location of the subducted Nazca Ridge. Symbols same as to the left. Panel A,A′ cross section showing event depths (in km) for events projected from area in red box on map. Red line indicates the slab surface from Antonijevic et al. (2015) and Wagner and Okal (2019). Right panel (B,B′) shows depth below sea level in km for the oceanic Moho (solid black line) and bathymetry (dotted line) across the Nazca Ridge from Contreras-Reyes et al. (2019).

less hydrated overall. However, side swath bathymetry surveys show evidence of trench parallel normal faults across both the Nazca Ridge and the adjacent normal oceanic plate with similar vertical offsets on the order of ∼200 m across our study area irrespective of crustal thickness (Hussong et al., 1988; Hagan and Moberly, 1994; Hampel et al., 2004; Kukowski et al., 2008). A more direct way to determine the hydration state of the oceanic plate is through tomographic modeling of seismic velocities. Wide-angle seismic studies north of the Nazca Ridge indicate average uppermost mantle velocities of ∼7.8 km/s, consistent with moderate hydration (Krabbenhoeft et al., 2004). However, along the ridge, somewhat higher uppermost mantle velocities are observed (∼8.0 km/s) consistent with an absence of mantle hydration (Contreras-Reyes et al., 2019), though the resolution of these studies at upper mantle depths is limited. Finally, Hu and Liu (2016) propose a slab tear as a possible cause for the observed absence in seismicity along the projected Nazca Ridge track based on geodynamic modeling and patterns of volcanism. However, given the clear evidence from seismic imaging for a continuous slab in this region from receiver functions (i.e., Bishop et al., 2017, 2018), teleseismic tomography (Scire et al., 2015), and surface wave tomography (Antonijevic et al., 2015, 2016), this explanation for the observed seismic gap is inconsistent with existing detailed imaging of the region.

METAMORPHIC IMPLICATIONS

Figure 2A shows a simplified schematic version of the cross section shown in **Figure 1** (A,A′) that we use to model our hypothesis. We assume the top of the oceanic crust is at the same depth along the transect, placing it at 70 km depth based on the depths of observed seismicity and the thickness of the overriding continental crust (Bishop et al., 2017). The base of the "normal" oceanic crust to either side of the ridge is assumed to be 77 km depth (assuming a 7 km thick crust) and the base of the Nazca Ridge crust is at 88 km depth (based on the 18 km crustal thickness imaged offshore). Here we show the penetration depth of water into the Nazca plate to also be 18 km beneath the surface of the oceanic crust (i.e., at 88 km depth), consistent with a number of previous studies investigating the depth of mantle hydration (e.g., Ranero et al., 2003; Contreras-Reyes et al., 2011;

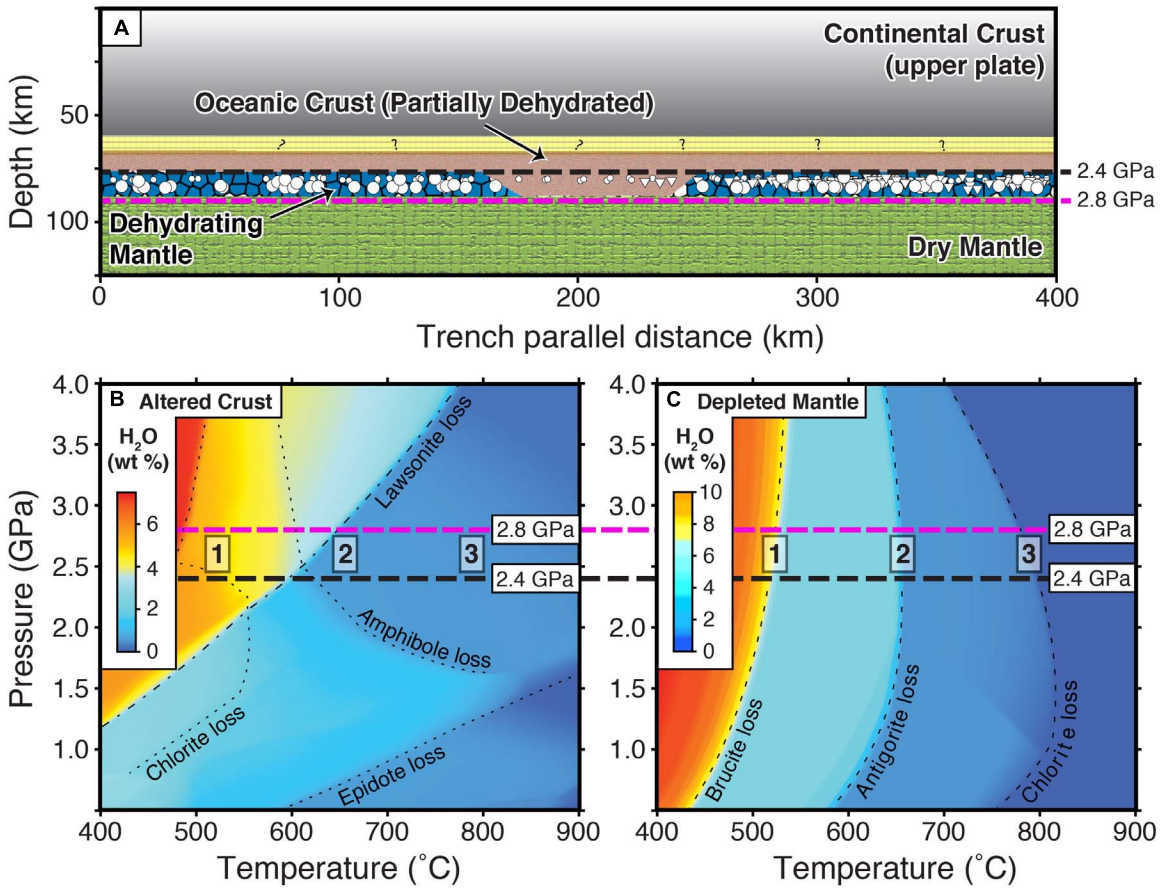

FIGURE 2 | Schematic diagram of our hypothesis: **(A)** Simplified trench-parallel cross section based on geometry shown in **Figure 1**. Section has been simplified so that the plate is perfectly flat across the interior 400 km (~150 km on either side of the ridge) and so that all seismicity is projected to the depth range of our proposed hydrated mantle lithosphere (lateral distribution still the same as in the cross section in **Figure 1**). Green region indicates dry oceanic mantle lithosphere. Blue indicates hydrated oceanic mantle lithosphere. White circles/triangles are seismic events (same symbols as in **Figure 1**). Light brown region is oceanic crust (MORB). Yellow region indicates possible mantle material trapped between the oceanic crust and the overlying continental crust (grayscale). Black dashed line is depth to the base of "normal" oceanic crust (i.e., top of hydrated mantle lithosphere). Magenta line is proposed maximum depth of hydration into the oceanic plate. **Bottom:** Mineralogically bound H_2O contents of hydrated MORB **(B)** and peridotite **(C)**, based on phase equilibria calculations. Dashed lines show pressures corresponding to lines of the same color in the cross section above. Boxes 1, 2, and 3 indicate regions where oceanic mantle undergoes significant dehydration at pressures experienced by hydrated mantle lithosphere. Versions of these diagrams labeled with the mineral assemblages associated with the H_2O contents are available in **Supplementary Information**.

Lefeldt et al., 2012). We note that in order for our model to hold, the penetration depth of water simply needs to be greater than normal oceanic crustal thickness, and less than or equal to the ridge crustal thickness. For clarity, we have projected seismicity from cross-section A,A′ (**Figure 1**) vertically to depths between the normal oceanic Moho and the maximum penetration depth of water into the slab. This allows us to demonstrate along-strike variability in intermediate depth seismicity, and is reasonable given that (a) the slab is unlikely to be perfectly horizontal along the cross section and (b) depth errors in hypocentral locations typically significantly exceed errors in latitude and longitude.

According to our hypothesis, the blue region in **Figure 2A** (hydrated mantle lithosphere) generates seismicity at these depths because it is undergoing dehydration reactions and the brown region (oceanic crust) is not dehydrating, and is therefore not generating seismicity. Because there is no hydrated mantle below the thick crust of the Nazca Ridge, there is a seismic gap. The discriminating region, then, lies between the 77 km depth of normal oceanic Moho (black dashed line in **Figure 2C**) and the assumed 88 km depth that marks the lowermost penetration depth of water into outer rise faults (magenta dashed line in **Figure 2C**). If our hypothesis is correct, the temperature of this region should correspond to a *P*/*T* condition at which hydrated peridotite would dehydrate but hydrated MORB would not, based on the assumption that temperature would be the same at these depths, regardless of whether the material is MORB or hydrated oceanic mantle lithosphere.

Figures 2B,C show the amount of structurally bound H_2O that can be incorporated into altered crust and depleted mantle, respectively. These diagrams are based on phase equilibria that were calculated for a composite crustal composition from DSDP sites 417 and 418 (Staudigel et al., 1989, 1996) and for harzburgitic

mantle (Ringwood, 1982). Sufficient H_2O was added to each bulk composition to saturate mineral assemblages at every *P*/*T* condition with fluid, and the amount of water contained in the coexisting mineral assemblage is contoured in **Figure 2** (see also Hacker, 2008, for water contents of a larger range of possible rock composition). Calculations utilized Perple_X (Connolly, 2005) and a 2004 update to the Holland and Powell (1998) thermodynamic dataset for mineral end-members. We used the suite of mineral solution models employed by Baxter and Caddick (2013), with the exception of updated models for antigorite (Padrón-Navarta et al., 2013) and amphibole and omphacite (Diener and Powell, 2012). Silicate melt was not considered. Calculated mineral assemblages are labeled in more detail in the **Supplementary Information**, where calculated densities of both rocks are also shown.

The dashed lines in **Figures 2B,C** correspond to the dashed lines of the same colors in **Figure 2A** – indicating the pressures at the base of the normal oceanic crust (∼2.4 GPa) and at the maximum penetration depth of water into the oceanic plate (∼2.8 GPa) as determined by converting the associated depths to pressures based on the Preliminary Reference Earth Model (PREM; Dziewonski and Anderson, 1981). We identify three temperature ranges within this pressure range at which hydrated peridotite releases a significant amount of water: ∼500°C upon the loss of brucite (box 1, **Figure 2C**), ∼640°C upon the loss of antigorite (box 2, **Figure 2C**) and ∼800°C upon chlorite breakdown (box 3, **Figure 2C**). We note that ∼640°C is similar to the temperature modeled for a flat slab at similar depth by van Hunen et al. (2002). If we then plot these same temperature boxes on the MORB phase diagram, we note that indeed, boxes 2 and 3 lie in regions at which MORB has already undergone extensive dehydration and is not dehydrating further, consistent with our hypothesis. Colder subduction that intersects box 1 would, however, be associated with crust that retains water in both lawsonite and amphibole.

According to our hypothesis, the oceanic crust along and adjacent to the subducted Nazca Ridge will be undergoing little dehydration by the time it reaches the *P*/*T* conditions of our seismic gap, implying that it has already fully dehydrated or that its H_2O content is sequestered in stable phases at these conditions. Subducting oceanic crust undergoes a sequence of dehydration reactions, but one of the most commonly attributed to the formation of intermediate depth seismicity is the breakdown of lawsonite (e.g., Kim et al., 2015; Okazaki and Hirth, 2016; Incel et al., 2017). In the Nazca Ridge case, this suggests that the oceanic crust must have exceeded the maximum temperatures of lawsonite (and amphibole) stability by the time the top of the slab reaches 70 km depth and the bottom of the hydrated layer of the slab reaches 88 km depth. Our hypothesis requires that off-ridge regions of thinner crust are still undergoing peridotite dehydration reactions at these same *P*/*T* conditions, which is true in **Figures 2B,C** for box 2 (dehydration of antigorite in the slab mantle) and box 3 (dehydration of chlorite in the slab mantle), but not box 1 (dehydration of brucite in the slab mantle that would be accompanied by dehydration of crust in the on-ridge section). Choosing whether peridotite dehydration at 640 or 800°C is most appropriate is more equivocal, given that the temperatures within regions of flat slab subduction are highly dependent on the three-dimensional geometry of the slab and the duration of time the overriding plate has been insulated from asthenospheric temperatures by the slab. Detailed time-dependent thermal modeling is required to better assess the implications of these predicted temperatures. However, either option demonstrates that our hypothesis is viable from a simplified petrologic perspective.

SEISMICITY PATTERNS ASSOCIATED WITH OTHER REGIONS OF SUBDUCTED THICK OCEANIC CRUST

Pampean Flat Slab

The most obvious and contrasting comparison to the lack of seismicity along the subducting Nazca Ridge along the Peruvian flat slab is the notable abundance of seismicity present along the subducting Juan Fernandez ridge along the Pampean flat slab in Chile and Argentina (**Figure 3**). Unlike the Nazca Ridge which is formed by a hot spot located along the Nazca-Pacific spreading center, the Juan Fernandez Ridge results from an intraplate hot-spot located 900 km from the South American margin (von Huene et al., 1997; Yañez et al., 2001, 2002). This means that, unlike the Nazca Ridge, there is no conjugate ridge to provide constraints on its projected location beyond the trench. It also means that unlike the Nazca Ridge, the Juan Fernandez ridge is not the same age as the surrounding plate – the oldest observed seamount close to the trench is ∼ 8.5 Ma, whereas the oceanic plate it sits on is ∼38 Ma (von Huene et al., 1997; Yañez et al., 2001; Mueller et al., 2008).

Reconstructions based on past plate motions indicate a major inflection point in the ridge track at 25 Ma coincident with the fracturing of the Farallon plate and the formation of the Nazca plate. This inflection point is believed to have subducted ∼11 Ma (Yañez et al., 2001) (white circles, **Figure 3**). Prior to that time, the Juan Fernandez Ridge would have been migrating southward along the Chilean margin much as the Nazca Ridge is migrating southward today. However, since 11 Ma, the ridge track and plate convergence directions have been nearly parallel, resulting in only a minor southward migration since the mid-Miocene (Yañez et al., 2001).

Over the past twenty years, a number of broadband seismic deployments (i.e., OVA99 and CHARSME (e.g., Marot et al., 2013), CHARGE (Beck et al., 2000); SIEMBRA (Beck and Zandt, 2007); ESP (Gilbert, 2008) have collected data above the projected location of the Juan Fernandez Ridge that have been used to constrain the geometry of the downgoing plate, and to relocate intermediate slab seismicity (e.g., Anderson et al., 2007; Marot et al., 2013; **Figure 3**). As was the case in Peru, the projected location of the subducted Juan Fernandez ridge coincides closely with the shallowest portion of the Pampean flat slab (Anderson et al., 2007). Unlike Peru, however, both global catalogs and local catalogs based on regional networks (i.e., Anderson et al., 2007; Marot et al., 2013) show the highest concentration of seismicity and moment release concentrated directly along the projected

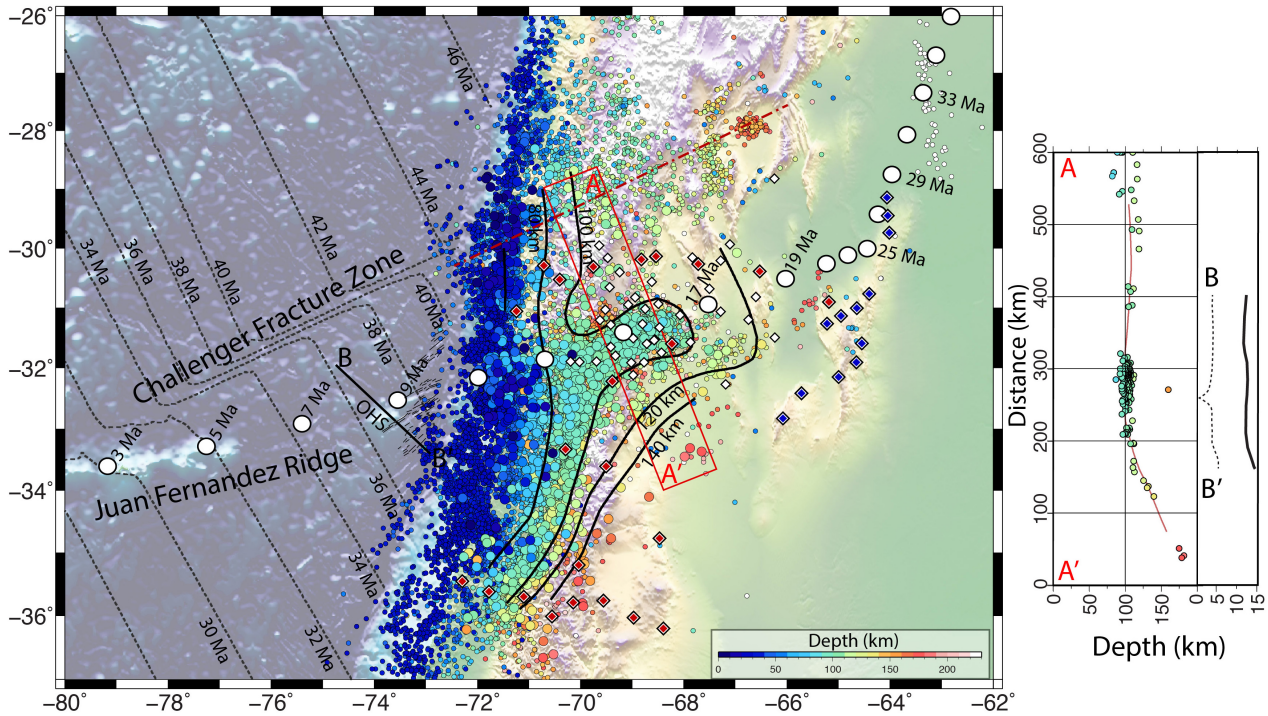

FIGURE 3 | Juan Fernandez Ridge subduction and earthquake distribution. **Left:** Map showing seismicity from the Reviewed International Seismological Center's earthquake catalog (1990–2017), with events shallower than 50 km removed east of –70°W for clarity. Large circles are hypocenters from Anderson et al. (2007) also with hypocenters shallower than 50 km removed east of –70°W. Offshore dashed lines show age contours from Mueller et al. (2008). Offshore solid black line shows the location panel B,B′ of the cross section from Kopp et al. (2004). Label "OHS" indicates the location of the O'Higgins seamount. Thin black lines offshore near the OHS indicate the locations of ridge-parallel normal faults from Ranero et al. (2005). White circles show projected track of the Juan Fernandez Ridge, along with ages of the seamount at those locations, from Yañez et al. (2001). Red diamonds, blue diamonds, and white diamonds show seismic station locations for the CHARGE, ESP, and SIEMBRA experiments, respectively. Dash-dot red line shows projected location of Challenger Fracture Zone. Solid black lines show slab contours from Anderson et al. (2007). Red rectangular box panel A,A′ shows area over which events were projected onto cross section to the right. **Right:** Cross-section panel A,A′ across the projected location of the subducted Juan Fernandez Ridge. Circles show event locations (depth in km) from Anderson et al. (2007), and red line shows top of slab from Anderson et al. (2007). Right panel (B,B′) shows depth below sea level in km for the oceanic Moho (solid black line) and bathymetry (dotted line) across the O'Higgins seamount from Kopp et al. (2004).

location of the Juan Fernandez Ridge. The right-hand panel of **Figure 3** (A,A′) shows the locations of intermediate depth earthquakes within 50 km of the roughly ridge-perpendicular cross section extending from (−28.8°S; −70.2°W) to (−33.8°S; −67.85°W). The red line plotted beneath the seismicity profile indicates the top of the subducted slab as determined by Anderson et al. (2007). As is the case in Peru, while some receiver function studies such as Gans et al. (2011) show evidence of the oceanic Moho in this region, the errors in the absolute depths locations of the receiver function are too great to allow an assessment of whether the observed seismicity is due to slab mantle or slab crustal processes.

To understand the cause of this seismicity, especially in contrast to the absence of seismicity along the Nazca Ridge, we again look at the structure of the downgoing oceanic plate, comparing the ridge track to normally subducted crust on either side. The age of the Nazca plate along the Chilean margin near the Juan Fernandez Ridge ranges from ∼34 to ∼40 Ma, becoming progressively older to the north (Mueller et al., 2008). Side swath bathymetry shows trench parallel normal faults close to the trench similar to the plate near the Nazca Ridge. These trench parallel normal faults associated with the downward bending of the oceanic plate are limited to an area within 30 km of the trench (Kopp et al., 2004; Ranero et al., 2005). However, these bathymetry studies also show extensive normal faults parallel to the Juan Fernandez ridge track that have no analog in Peru (**Figure 3**; von Huene et al., 1997; Kopp et al., 2004; Ranero et al., 2005). These ridge-parallel faults are particularly pronounced, with some such as the O'Higgins Fracture extending over 100 km across the oceanic plate (Kopp et al., 2004). A M_w = 6.7 normal fault earthquake occurred on April 9, 2001 that likely ruptured along the O'Higgins Fracture zone with northeast-southwest striking nodal planes (Fromm et al., 2006). This earthquake and aftershock sequence was relocated with data from seismic stations on-shore and the aftershocks extended to a depth of ∼25–30 km suggesting that outer-rise normal faults can rupture through the oceanic crust and into the mantle lithosphere (Fromm et al., 2006).

Wide angle seismic refraction profiles provide excellent constraints on the structure of the oceanic crust and mantle in the vicinity of the Juan Fernandez Ridge. Orthogonal survey lines across the O'Higgins Seamount at the eastern end of the

ridge indicate only modest crustal thickening (8–10 km thick crust) beneath the highest elevations of the seamount (Kopp et al., 2004), though the receiver function study of Gans et al. (2011) argues that the oceanic crust currently located within the horizontal portion of the subducted slab is at least 13 km thick locally. Velocity modeling of the oceanic crust and mantle across the region shows evidence for reduced crustal and upper mantle velocities (Kopp et al., 2004; Contreras-Reyes et al., 2014, 2015; Moscoso and Grevemeyer, 2015). Kopp et al. (2004) indicate that hydration beneath the O'Higgins Seamount Group likely extends at least 6 km below the Moho, indicating a total hydration thickness of 16–18 km. This hydration is likely enhanced by the presence of extensive ridge-parallel normal faulting, whose spatial extent is similar to the area of low upper mantle velocities (Kopp et al., 2004; Contreras-Reyes et al., 2015).

Taken together, these data suggest that the Juan Fernandez Ridge has a much less extensive crustal root than the Nazca Ridge, and that trench parallel and perpendicular faulting has produced extensive hydration of the mantle lithosphere beneath the ridge that can explain intermediate depth seismicity on the projected location of the Juan Fernandez Ridge. This leaves outstanding the question of why intermediate depth seismicity is more pronounced along the projected Juan Fernandez Ridge track than in adjacent areas with more normal oceanic crust. One possible explanation could be the ridge-parallel faulting that is largely confined to the region close to the ridge itself (e.g., Ranero et al., 2005). Another possible explanation could be related to enhanced bending related stresses due to the contortion necessary to accommodate the abrupt along-strike transition (from north to south) from flat slab to normally dipping slab. Recent work by Sandiford et al. (2019) attributed bending related stresses to increases in seismicity at the hinge zones of the northern Peruvian flat slab and the Mexican flat slab. A similar, but trench perpendicular, bending geometry might be able to explain the high concentration of seismicity along the subducted Juan Fernandez Ridge. Finally, we note that because the Juan Fernandez Ridge has been subducting beneath the same part of the South American continent for ∼11 Ma, it is likely to be colder than the corresponding portion of the southward progressing Nazca Ridge due to the greater amount of time the overriding continent has been isolated from asthenospheric corner flow (van Hunen et al., 2002). Based on the phase diagrams in **Figure 2**, MORB compositions at temperatures below 640°C would still contain a significant amount of water, particularly in the form of lawsonite, and are therefore still capable of dehydration reactions that might produce the observed seismicity.

Cocos and Carnegie Ridges

The Cocos and Carnegie Ridges are structurally much more similar to the Nazca Ridge than the Juan Fernandez Ridge. Both ridges formed at the Galapagos hot spot near the plate boundary no earlier than at the time of the fracturing of the Farallon plate and the formation of the Cocos and Nazca plates (∼23 Ma) (Lonsdale, 2005). The Cocos ridge crust is ∼18.5–20 km thick (Sallares et al., 2003; Walther, 2003), thinning at the flanks to ∼8–10 km thick (Walther, 2003). Sallares et al. (2003) do not indicate any resolution below the oceanic Moho. Walther (2003) argues that Pn velocities indicate low uppermost mantle velocities at the flanks (7.8 km/s) that appear to decrease below the thickest portions of the crust. However, because of a lack of apparent density decrease, Walther (2003) suggests the decrease in velocity is not likely due to hydration but rather to an imperfect separation of basaltic melt and residual mantle peridotite during ridge formation. Adjacent regions north of the Cocos ridge indicate mantle hydration up to 10 km below the oceanic Moho (Ranero et al., 2003; Lefeldt et al., 2012). Unlike the Nazca Ridge, however, while adjacent regions show evidence of significant outer rise faulting (Ranero et al., 2003), there is limited – to – no evidence of outer rise faulting along the Cocos Ridge (e.g., von Huene et al., 2000).

The Carnegie Ridge crustal structure is similar to that of the Cocos Ridge. Its crustal thickness ranges from 14 to 19 km (e.g., Graindorge et al., 2004; Sallares et al., 2005; Gailler et al., 2007; Collot et al., 2017), but no robust estimates of sub-ridge Moho velocities are available at this time. The Carnegie Ridge, however, does show some evidence from bathymetry and seismic surveys for trench-parallel normal faulting in the oceanic plate, at least along the northern flanks of the ridge (Marcaillou et al., 2016).

Seismic gaps have been noted along both the Cocos (e.g., Husen et al., 2003; Peacock et al., 2005) and Carnegie (e.g., Gutscher et al., 1999a; Font et al., 2013; Yepes et al., 2016; Rosenbaum et al., 2018) ridges (**Figure 4**). Intermediate depth seismicity in the downgoing Cocos plate decreases in volume and maximum depth from northwest to southeast (cross-section C,C′ showing seismicity within 75 km of 11°N, −85.9°W to 8.3°N, −81°W, **Figure 4**) leading up to the projected location of the Cocos ridge. The Cocos Ridge is just west of the seismically active Panama Fracture Zone (PFZ) whose north-south band of seismicity appears to continue past the trench up to its projected intersection point with the Cocos ridge, though little of this seismicity extends below 50 km depth. The absence of seismicity east of the east-west trending Carnegie Ridge is complicated by its projected intersection with the Grijalva Fracture Zone (Lonsdale, 2005; Yepes et al., 2016) which comprises the southern flank of the Nazca-Cocos rift zone. Seismicity is ample and extends to over 200 km depth for locations south of the Grijalva Fracture zone (cross-section A,A′ showing seismicity within 75 km of 1.9°N, −77.7°W to −3.8°S, −78.7°W), but is notably absent at depths below 50 km to the north along the projected location of the Carnegie Ridge. While the geometry of the slab between the Grijalva Fracture zone and central Colombia is not well defined by Wadati-Benioff zone seismicity, it has been postulated that slab tears may help accommodate rapid changes in slab geometry and the subduction of the Carnegie ridge (Gutscher et al., 1999a; Yepes et al., 2016; Rosenbaum et al., 2018).

Broadly speaking, the combination of a subducting thick oceanic crust that is coincident with a gap in intermediate depth seismicity for both the Cocos and Carnegie ridges is consistent and supportive of our hypothesis. However, there are several possible potentially confounding tectonic factors. First, for both ridges, the age of the oceanic plate increases rapidly away from the ridge in the direction of increased seismicity. Given the comparatively young age of the oceanic plate along these ridges (14–18 Ma (Mueller et al., 2008), and the even

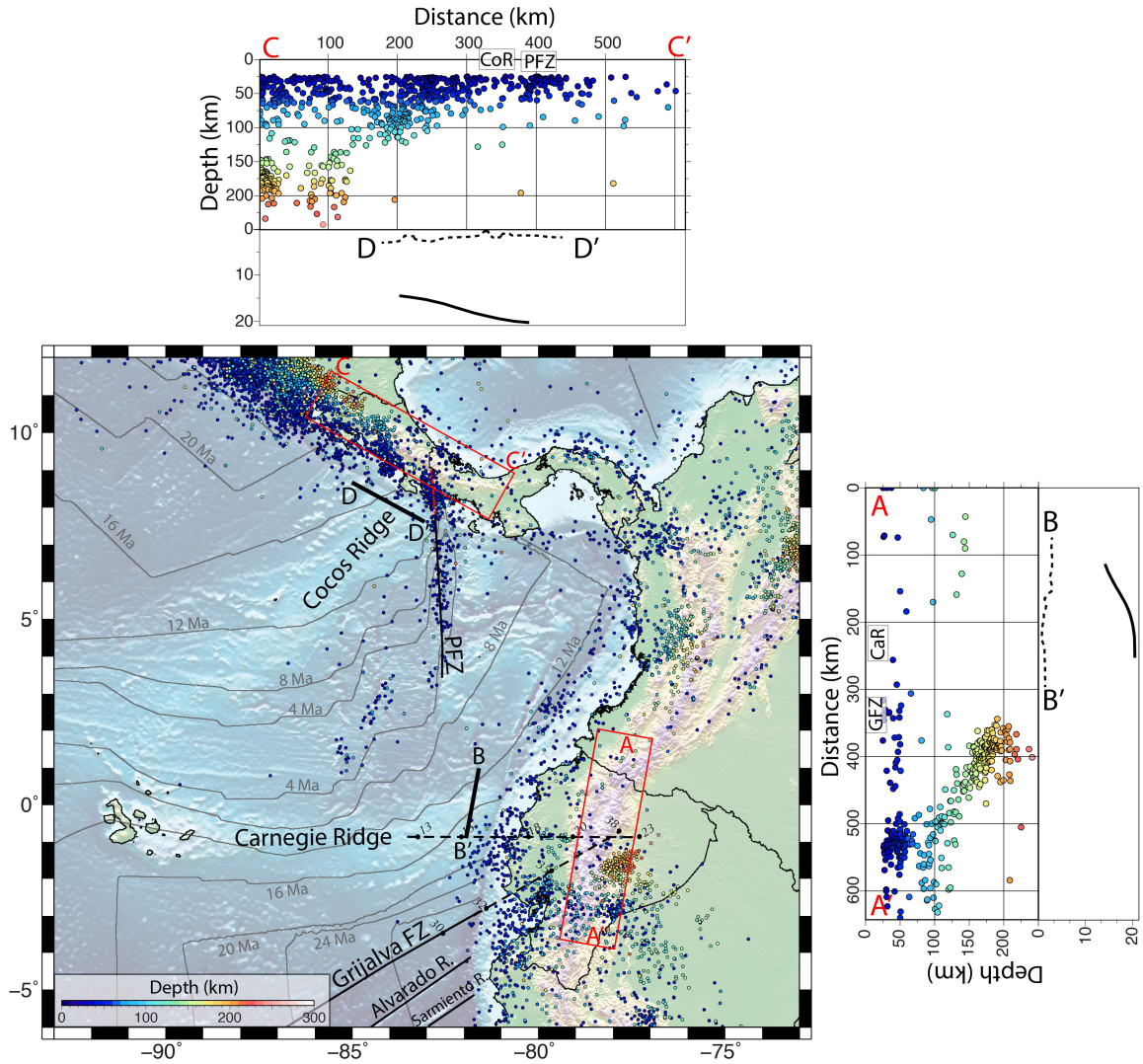

FIGURE 4 | Carnegie and Cocos Ridge subduction and earthquake distribution. **Left:** Map showing seismicity from the Reviewed International Seismological Center's earthquake catalog (1990–2017) as small circles. Offshore gray lines show age contours from Mueller et al. (2008). Offshore solid black line across the Carnegie Ridge shows the location panel B,B′ of the cross section from Sallares et al. (2005). Offshore solid black line across the Cocos Ridge shows the location panel D,D′ of the cross section from Sallares et al. (2003). Black dashed lines and italic numbers show the projected Carnegie Ridge and Grijalva Fracture Zone locations and ages from Lonsdale (2005). Dash-dot red line shows projected location of the Panama Fracture Zone. Red rectangular box panel A,A′ shows area over which events were projected onto cross section to the right. **Right:** Cross-section panel A,A′ across the projected location of the subducted Carnegie Ridge. Circles show projected event locations (depth in km) from the Reviewed ISC catalog (1990–2017). Left panel (B,B′) shows depth below sea level in km for the oceanic Moho (solid black line) and bathymetry (dotted line) across the Carnegie ridge from Sallares et al. (2005). **Top:** Cross-section panel C,C′ across the projected location of the subducted Cocos Ridge. Circles show projected event locations (depth in km) from the Reviewed ISC catalog (1990–2017). Lower panel (D,D′) shows depth below sea level in km for the oceanic Moho (solid black line) and bathymetry (dotted line) across the Carnegie ridge from Sallares et al. (2003).

younger ages on the sides of the ridges with less seismicity (<12 Ma), it is possible that a significant portion of the observed patterns are due to the younger plates being too warm to stay hydrated much deeper than 50 km. Secondly, because there is no conjugate to these ridges that is not currently being subducted, it is difficult to know how much of the ridge has actually been subducted, and whether either ridge extends far enough landward from the trench to be responsible for the observed gaps. Estimates from the timing of first subduction for the Cocos Ridge range from 8 to 1 Ma, though many prefer ages of <3 Ma (e.g., Protti et al., 1994; Kolarsky et al., 1995; von Huene et al., 2000; MacMillan et al., 2004; Dzierma et al., 2011; Morell et al., 2012) which would extend the Cocos Ridge as far landward as the former arc, but not much farther ENE. For the Carnegie Ridge, if ridge formation began at 23 Ma with the breakup of the Farallon plate, onset of ridge subduction would have started 6–8 Ma (Lonsdale, 2005). However, this is far from certain, and other estimates suggest that there is little evidence for subduction of the Carnegie Ridge prior to 5 Ma (e.g., Bourdon et al., 2003; Michaud et al., 2009). The abundance

of volcanic arc activity suggests that flat slab subduction that might be associated with the downgoing Carnegie Ridge must be relatively recent. A number of studies point to petrological changes along the arc to suggest that a shallowly subducting Carnegie Ridge may affect arc magmatism at the surface, either by affecting the depth of melting (e.g., Chiaradia et al., 2020) or through the melting of overthickened oceanic crust due to adjacent tears in the downgoing plate (e.g., Gutscher et al., 1999a; Bourdon et al., 2003; Rosenbaum et al., 2018). One way or the other, 5 Ma of subduction would still imply a substantial amount of subducted ridge, certainly sufficient to be responsible for the observed seismic gap within uncertainties. Finally, because both the Cocos and Carnegie ridges are intercepted by fracture zones, associated tears or slab windows could result in changes in the thermal structures of the adjacent subduction zone that could affect not only arc volcanism, but also the dehydration reactions responsible for observed seismicity patterns (e.g., Gutscher et al., 1999a; Bourdon et al., 2003; Dzierma et al., 2011; Rosenbaum et al., 2018). For these reasons, without further data, we must consider these ridges consistent with, but not necessarily supportive of, our hypothesis.

DISCUSSION

The nature of the relationship (if any) between oceanic crustal structures and intermediate/deep seismicity has long been discussed. For example, Kirby et al. (1996) consider the relationship between the "mechanically flawed and heterogeneous lithosphere" and intermediate depth seismicity. In particular, they note the effects of fractures, both from outer-rise faults and fracture zones on the hydration of the oceanic lithosphere and associated potential for increased intermediate depth seismicity. We note that similar patterns are visible in all of our study areas along the projected locations of the Nazca Fracture Zone, Challenger Fracture Zone, Grijalva Fracture Zone, and Panama Fracture Zone for the study areas near the Nazca, Juan Fernandez, Carnegie, and Cocos ridges, respectively. However, to our knowledge, we are the first to suggest that the presence of overthickened oceanic crust can result in an absence of intermediate depth seismicity if crustal thickness exceeds the maximum penetration depth of water into the subducted plate. Kirby et al. (1996) do mention the role of ridges in the formation of seismicity, and while they note the apparent absence or dearth of seismicity associated with the Nazca, Cocos, Carnegie and D'Entrecasteaux ridges, they focus instead on the overabundance of seismicity present along the Juan Fernandez Ridge.

We would argue that the Juan Fernandez Ridge is fundamentally different from the type of ridge we would expect to produce a gap in intermediate depth seismicity, both because of its limited crustal root and because of its extensive ridge-parallel faulting. Interestingly, these structures may be related to the location and timing of ridge emplacement – the Juan Fernandez Ridge is the only one considered here that did not form at or near a spreading center. This may affect the architecture of the crust in important ways. The Juan Fernandez Ridge crustal thickness is primarily due to increases in upper crustal layers, but a relatively constant thickness lower crust (e.g., Kopp et al., 2004). In contrast, the Nazca, Carnegie, and Cocos ridges all attained their increased Moho depths through thickening of the lower crust, with little to no increase in the thicknesses of layers in the upper crust (e.g., Sallares et al., 2003; Krabbenhoeft et al., 2004; Sallares et al., 2005; Contreras-Reyes et al., 2019). An intriguing analog to the Juan Fernandez Ridge might be the Louisville Ridge on the Pacific plate that also formed at an intraplate hotspot (the Louisville hotspot, Watts et al., 1988). Here, as with the Juan Fernandez Ridge, most of the additional crustal volume is added intrusively into the upper crust with only modest variations in lower crustal thickness (Contreras-Reyes et al., 2010; Robinson et al., 2018). However, unlike the Juan Fernandez Ridge, there is no evidence of ridge-parallel fracturing or hydration of the mantle beneath the ridge itself (Contreras-Reyes et al., 2010). While the Louisville Ridge has been associated with a reduction in seismicity at shallow to intermediate depths (Giardini and Woodhouse, 1984; Habermann et al., 1986; Scholtz and Small, 1997), the seismicity pattern is less clear in part due to the oblique subduction of the ridge, and uncertainty about its projected location. More work is needed to understand how crustal thickening mechanisms, Moho depth, and seismicity patterns are related in this region.

At this stage, we know of no example that contradicts our hypothesis that if the oceanic crust is thicker than the maximum penetration depth of water into the slab, intermediate depth seismicity will be reduced or absent. The precise mechanism by which dehydration results in intermediate depth seismicity, whether it be by traditional "dehydration embrittlement" via an increase in pore pressure, by the formation of nanocrystalline/fine grained dehydration products or fault plane weakening, by DDST, or some combination of the above, may depend on the precise P/T conditions of the subducting slab, and is certainly a field of ongoing scientific research. Our hypothesis does, however, strongly suggest that dehydration plays a dominant role in the generation of intermediate depth seismicity, even if the precise mechanism remains uncertain.

For future work, more information is needed on the crust and mantle structures of subducting bathymetric features. Better constraints on the depth of hydration at trench outer-rise settings, both in regions with and without overthickened crust will dramatically improve our understanding of the role of slab mantle hydration on the genesis of intermediate depth seismicity. If our hypothesis is true, then intermediate depth seismicity adjacent to seismic gaps like the one in Peru can be used as a virtual thermometer to provide direct evidence of the temperature at a specific range of depths within a subducting plate at significant distance from the trench. These types of constraints could prove very valuable as ground truth for geodynamic models of subduction zone thermal structures.

DATA AVAILABILITY STATEMENT

Publicly available datasets were analyzed in this study. This data can be found here: https://doi.org/10.31905/D808B830, http://www.isc.ac.uk/iscbulletin/search/catalogue/.

AUTHOR CONTRIBUTIONS

LW is responsible for the original content and initial manuscript of this work. MC provided the Perplex modeling and contributions to the metamorphic petrology portions of this manuscript. LW, ML, and SB led the collection of the PULSE dataset. SB and LW were leaders in the collection of the CAUGHT dataset. SB, AK, and ML contributed to discussions and revisions of the manuscript. All authors read and approved the submitted version.

FUNDING

SB's contribution to this work was supported by NSF grant EAR 1723065.

ACKNOWLEDGMENTS

Thanks are due to Geoff Abers, Greg Hirth, and many others for insightful discussions and support for this manuscript. Many thanks to George Zandt for his leadership on the CAUGHT deployment and for all of his support and helpful suggestions over the years. We thank our reviewers for their constructive comments and the editor, VM, for his support of this manuscript.

SUPPLEMENTARY MATERIAL

The Supplementary Material for this article can be found online at: https://www.frontiersin.org/articles/10.3389/feart.2020.00244/full#supplementary-material

REFERENCES

Abers, G. A., Nakajima, J., van Keken, P. E., Kita, S., and Hacker, B. R. (2013). Thermal–petrological controls on the location of earthquakes within subducting plates. *Earth Planet. Sci. Lett.* 369, 178–187. doi: 10.1016/j.epsl.2013.03.022

Anderson, M., Alvarado, P., Zandt, G., and Beck, S. (2007). Geometry and brittle deformation of the subducting Nazca Plate, central Chile and Argentina. *Geophys. J. Int.* 171, 419–434. doi: 10.1111/j.1365-246x.2007.03483.x

Antonijevic, S. K., Wagner, L. S., Beck, S. L., Long, M. D., Zandt, G., and Tavera, H. (2016). Effects of change in slab geometry on the mantle flow and slab fabric in Southern Peru. *J. Geophys. Res.* 121, 7252–7270. doi: 10.1002/2016jb013064

Antonijevic, S. K., Wagner, L. S., Kumar, A., Beck, S. L., Long, M. D., Zandt, G., et al. (2015). The role of ridges in the formation and longevity of flat slabs. *Nature* 524, 212–215. doi: 10.1038/nature14648

Baxter, E. F., and Caddick, M. J. (2013). Garnet growth as a proxy for progressive subduction zone dehydration. *Geology* 41, 643–646. doi: 10.1130/g34004.1

Beck, S. L., Wallace, T., and Zandt, G. (2000). *Slab Geometry in the Southern Andes. International Federation of Digital Seismograph Networks. Dataset/Seismic Network.* doi: 10.7914/SN/YC_2000

Beck, S. L., and Zandt, G. (2007). *Lithospheric Structure and Deformation of the Flat Slab Region of Argentina. International Federation of Digital Seismograph Networks. Dataset/Seismic Network*. doi: 10.7914/SN/ZL_2007

Beck, S. L., Zandt, G., and Wagner, L. S. (2010). *Central Andean Uplift and the Geodynamics of the High Topography. International Federation of Digital Seismograph Networks. Dataset/Seismic Network*. doi: 10.7914/SN/ZG_2010

Bishop, B., Beck, S. L., Zandt, G., Wagner, L. S., Long, M. D., Antonijevic, S. K., et al. (2017). Causes and consequences of flat-slab subduction in southern Peru. *Geosphere* 13, 1392–1407. doi: 10.1130/GES01330.1

Bishop, B., Beck, S. L., Zandt, G., Wagner, L. S., Long, M. D., and Tavera, H. (2018). Foreland uplift during flat subduction: insights from the Peruvian Andes and Fitzcarrald Arch. *Tectonophysics* 73, 73–84. doi: 10.1016/j.tecto.2018.03.005

Bloch, W., John, T., Kummerow, J., Salazar, P., Krüger, O. S., and Shapiro, S. A. (2018). Watching dehydration: seismic indication for transient fluid pathways in the oceanic mantle of the subducting Nazca slab. *Geochem. Geophys. Geosyst.* 19, 3189–3207. doi: 10.1029/2018gc007703

Boneh, Y., Schottenfels, E., Kwong, K., van Zelst, I., Tong, X., Eimer, M., et al. (2019). Intermediate-depth earthquakes controlled by incoming plate hydration along bending-related faults. *Geophys. Res. Lett.* 46, 3688–3697. doi: 10.1029/2018gl081585

Bourdon, E., Eissen, J.-P., Gutscher, M.-A., Monzier, M., Hall, M. L., and Cotton, J. (2003). Magmatic response to early aseismic ridge subduction: the Ecuadorian margin case (South America). *Earth Planet Sci. Lett.* 205, 123–138. doi: 10.1016/s0012-821x(02)01024-5

Cai, C., Wiens, D. A., Shen, W., and Eimer, M. (2018). Water input into the Mariana subduction zone estimated from ocean-bottom seismic data. *Nature* 563, 389–394. doi: 10.1038/s41586-018-0655-4

Chernak, L. J., and Hirth, G. (2010). Deformation of antigorite serpentinite at high temperature and pressure. *Earth Planet. Sci. Lett.* 296, 23–33. doi: 10.1016/j.epsl.2010.04.035

Chernak, L. J., and Hirth, G. (2011). Syndeformational antigorite dehydration produces stable fault slip. *Geology* 39, 847–850. doi: 10.1130/g31919.1

Chiaradia, M., Müntener, O., and Beate, B. (2020). Effects of aseismic ridge subduction on the geochemistry of frontal arc magmas. *Earth Planet. Sci. Lett.* 531:115984. doi: 10.1016/j.epsl.2019.115984

Collot, J.-Y., Sanclemente, E., Nocquet, J.-M., Leprêtre, A., Ribodetti, A., Jarrin, P., et al. (2017). Subducted oceanic relief locks the shallow megathrust in central Ecuador. *J. Geophys. Res.* 122, 3286–3305. doi: 10.1002/2016JB013849

Connolly, J. A. D. (2005). Computation of phase equilibria by linear programming: a tool for geodynamic modeling and its application to subduction zone decarbonation. *Earth Planet. Sci. Lett.* 236, 524–541. doi: 10.1016/j.epsl.2005.04.033

Contreras-Reyes, E., Becerra, J., Kopp, H., Reichert, C., and Diaz-Naveas, J. (2014). Seismic structure of the north-central Chilean convergent margin: subduction erosion of a paleomagnetic arc. *Geophys. Res. Lett.* 41, 1523–1529. doi: 10.1002/2013gl058729

Contreras-Reyes, E., Grevemeyer, I., Watts, A. B., Flueh, E. R., Peirce, C., Moeller, S., et al. (2011). Deep seismic structure of the Tonga subduction zone: implications for mantle hydration, tectonic erosion, and arc magmatism. *J. Geophys. Res.* 116:2011JB008434. doi: 10.1029/2011JB008434

Contreras-Reyes, E., Grevemeyer, I., Watts, A. B., Planert, L., Flueh, E. R., and Peirce, C. (2010). Crustal intrusion beneath the Louisville hotspot track. *Earth Planet. Sci. Lett.* 289, 323–333. doi: 10.1016/j.epsl.2009.11.020

Contreras-Reyes, E., Muñoz-Linford, P., Cortes-Rivas, V., Bello-Gonzales, J. P., Ruiz, J. A., and Krabbenhoeft, A. (2019). Structure of the collision zone between the Nazca Ridge and the Peruvian convergent margin: geodynamic and seismotectonic implications. *Tectonics* 38, 3416–3435. doi: 10.1029/2019TC005637

Contreras-Reyes, E., Ruiz, J. A., Becerra, J., Kopp, H., Reichert, C., Maksymowicz, A., et al. (2015). Structure and tectonics of the central Chilean margin (31 – 33 S): implications for subduction erosion and shallow crustal seismicity. *Geophys. J. Int.* 203, 776–791. doi: 10.1093/gji/ggv309

DeMets, C., Gordon, R. G., and Argus, D. F. (2010). Geologically current plate motions. *Geophys. J. Int.* 181, 1–80. doi: 10.1111/j.1365-246x.2009.04491.x

Diener, J. F. A., and Powell, R. (2012). Revised activity–composition models for clinopyroxene and amphibole. *J. Metamorph. Geol.* 30, 131–142. doi: 10.1111/j.1525-1314.2011.00959.x

Dobson, D. P., Meredith, P. G., and Boon, S. A. (2002). Simulation of subduction zone seismicity by dehydration of serpentine. *Science* 298, 1407–1410. doi: 10.1126/science.1075390

Dzierma, Y., Rabbel, W., Thorwart, M. M., Flueh, E. R., Mora, M. M., and Alvarado, G. E. (2011). The steeply subducting edge of the Cocos Ridge: evidence from receiver functions beneath the northern talamanca range, south-central Costa Rica. *Geochem. Geophy. Geosys.* 12:3477. doi: 10.1029/2010GC003477

Dziewonski, A. M., and Anderson, D. L. (1981). Preliminary reference Earth model. *Phys. Earth Planet. Int.* 25, 297–356. doi: 10.1016/0031-9201(81)90046-7

Ferrand, T. P. (2019). Seismicity and mineral destabilizations in the subducting mantle up to 6 GPa, 200 km depth. *Lithos* 334, 205–230. doi: 10.1016/j.lithos.2019.03.014

Ferrand, T. P., Hilairet, N., Incel, S., Deldicque, D., Labrousse, L., Gasc, J., et al. (2017). Dehydration-driven stress transfer triggers intermediate-depth earthquakes. *Nat. Commun.* 8:15247.

Font, Y., Segovia, M., Vaca, S., and Theunissen, T. (2013). Seismicity patterns along the Ecuadorian subduction zone: new constraints from earthquake location in a 3-D a priori velocity model. *Geophys. J. Int.* 193, 263–286. doi: 10.1093/gji/ggs083

Fromm, R., Alvarado, P., Beck, S. L., and Zandt, G. (2006). The April 9, 2001 Juan Fernández Ridge (Mw 6.7) tensional outer-rise earthquake and its aftershock sequence. *J. Seismol.* 10, 163–170. doi: 10.1007/s10950-006-9013-3

Gailler, A., Charvis, P., and Flueh, E. R. (2007). Segmentation of the Nazca and South American plates along the Ecuador subduction zone from wide angle seismic profiles. *Earth Planet. Sci. Lett.* 260, 444–464. doi: 10.1016/j.epsl.2007.05.045

Gans, C. R., Beck, S. L., Zandt, G., Gilbert, H., Alvarado, P., Anderson, M., et al. (2011). Continental and oceanic crustal structure of the Pampean flat slab region, western Argentina, using receiver function analysis: new high-resolution results. *Geophys. J. Int.* 186, 45–58. doi: 10.1111/j.1365-246x.2011.05023.x

Gasc, J., Hilairet, N., Yu, T., Ferrand, T., Schubnel, A., and Wang, Y. (2017). Faulting of natural serpentinite: Implications for intermediate-depth seismicity. *Earth Plant. Sci. Lett.* 474, 138–147. doi: 10.1016/j.epsl.2017.06.016

Gasc, J., Schubnel, A., Brunet, F., Guillon, S., Mueller, H. J., and Lathe, C. (2011). Simultaneous acoustic emissions monitoring and synchrotron X-ray diffraction at high pressure and temperature: Calibration and application to serpentinite dehydration. *Phys. Earth Planet Int.* 189, 121–133. doi: 10.1016/j.pepi.2011.08.003

Giardini, D., and Woodhouse, J. H. (1984). Deep seismicity and modes of deformation in Tonga subduction zone. *Nature* 307, 505–509. doi: 10.1038/307505a0

Gilbert, H. (2008). *Eastern Sierras Pampeanas, Lithospheric Structure Above the Variably Dipping Nazca Slab. International Federation of Digital Seismograph Networks. Dataset/Seismic Network*. doi: 10.7914/SN/XH_2008

Graindorge, D., Calahorrano, A., Charvis, P., Collot, J.-Y., and Bethoux, N. (2004). Deep structures of the Ecuador convergent margin and the Carnegie Ridge, possible consequence on great earthquakes recurrence interval. *Geophys. Res. Lett.* 31:e018803. doi: 10.1029/2003GL018803

Green, H. W., and Houston, H. (1995). The mechanics of deep earthquakes. *Annu. Rev. Earth Planet. Sci.* 23, 169–213.

Grevemeyer, I., Ranero, C. R., and Ivandic, M. (2018). Structure of oceanic crust and serpentinization at subduction trenches. *Geosphere* 14, 395–410. doi: 10.1130/GES01537.1

Gutscher, M. A., Malavielle, J., Lallemand, S., and Collot, J.-Y. (1999a). Tectonic segmentation of the North Andean margin: impact of the Carnegie Ridge collision. *Earth Planet Sci. Lett.* 168, 255–270. doi: 10.1016/s0012-821x(99)00060-6

Gutscher, M. A., Olivet, J.-L., Aslanian, D., Eissen, J.-P., and Maury, R. (1999b). The "lost Inca Plateau": cause of flat subduction beneath Peru. *Earth Planet. Sci. Lett.* 171, 335–341. doi: 10.1016/s0012-821x(99)00153-3

Habermann, R. E., McCann, W. R., and Perin, B. (1986). Spatial seismicity variations along convergent plate boundaries. *Geophys. J. R. Astr. Soc.* 85, 43–68. doi: 10.1111/j.1365-246x.1986.tb05171.x

Hacker, B. R. (2008). H_2O subduction beyond arcs. *Geochem. Geophys. Geosyst.* 9:Q03001. doi: 10.1029/2007GC001707

Hacker, B. R., Peacock, S. M., Abers, G. A., and Holloway, S. D. (2003). Subduction factory -2. Are intermediate-depth earthquakes in subducting slabs linked to metamorphic dehydration reactions? *J. Geophys. Res.* 108:1129. doi: 10.1029/2001JB001129

Hagan, R. A., and Moberly, R. (1994). Tectonic effects of a subducting aseismic ridge: the subduction of the Nazca Ridge at the Peru trench. *Mar. Geophys. Res.* 16, 145–161. doi: 10.1007/bf01224757

Hampel, A. (2002). The migration history of the Nazca Ridge along the Peruvian active margin: a re-evaluation. *Earth Planet. Sci Lett.* 203, 665–679. doi: 10.1016/s0012-821x(02)00859-2

Hampel, A., Kukowski, N., Bialas, J., Huebscher, C., and Heinbockel, R. (2004). Ridge subduction at an erosive margin: the collision zone of the Nazca Ridge in southern Peru. *J. Geophys. Res.* 109:B02101. doi: 10.1029/2003JB002593

Holland, T. J. B., and Powell, R. (1998). An internally consistent thermodynamic data set for phases of petrological interest. *J. Metamorph. Geol.* 16, 309–343. doi: 10.1111/j.1525-1314.1998.00140.x

Hu, J., and Liu, L. (2016). Abnormal seismological and magmatic processes controlled by the tearing South American flat slabs. *Earth Planet Sci. Lett.* 450, 40–51. doi: 10.1016/j.epsl.2016.06.019

Husen, S., Quintero, R., Kissling, E., and Hacker, B. (2003). Subduction-zone structure and magmatic processes beneath Costa Rica constrained by local earthquake tomography and petrological modelling. *Geophys. J. Int.* 155, 11–32. doi: 10.1046/j.1365-246x.2003.01984.x

Hussong, D. M., Reed, T. B., and Bartlett, W. A. (1988). "SeaMarc II sonar imagery and bathymetry of the Nazca Plate and Peru forearc, ODP Leg 112," in *Proceedings of the ODP, Init. Repts., 112*, College Station, TX.

Incel, S., Hilairet, N., Labrousse, L., John, T., Deldicque, D., Ferrand, T., et al. (2017). Laboratory earthquakes triggered during eclogitization of lawsonite-bearing blueschist. *Earth Planet. Sci. Lett.* 459, 320–331. doi: 10.1016/j.epsl.2016.11.047

International Seismological Centre (2019). *On-Line Bulletin*. Thatcham: International Seismological Centre. doi: 10.31905/D808B830

John, T., Medvedev, S., Rüpke, L. H., Andersen, T. B., Podladchikov, Y. Y., and Austrheim, H. (2009). Generation of intermediate-depth earthquakes by self-localizing thermal runaway. *Nat. Geosci.* 2, 137–140. doi: 10.1038/ngeo419

Jung, H., Green, H., and Dobrzhinetskaya, L. (2004). Intermediate-depth earthquake faulting by dehydration embrittlement with negative volume change. *Nature* 428, 545–549. doi: 10.1038/nature02412

Kelemen, P. B., and Hirth, G. (2007). A periodic shear-heating mechanism for intermediate-depth earthquakes in the mantle. *Nature* 446, 787–790. doi: 10.1038/nature05717

Kim, D., Katayama, I., Wallis, S., Michibayashi, K., Miyake, A., Seto, Y., et al. (2015). Deformation microstructures of glaucophane and lawsonite in experimentally deformed blueschists: implications for intermediate-depth intraplate earthquakes. *J. Geophys. Res. Solid Earth* 120, 1229–1242. doi: 10.1002/2014jb011528

Kirby, S. (1995). Interslab earthquakes and phase changes in subducting lithosphere. *Rev. Geophys.* 33, 287–297.

Kirby, S. H., Engdahl, E. R., and Dehlinger, R. (1996). Intermediate depth intraslab earthquakes amd arc volcanism as physical expressions of crustal and uppermost mantle in subducting slabs. *Subduct. Top Bottom Geophys. Monogr. Ser.* 96, 347–355.

Kolarsky, R. A., Mann, P., and Monetero, P. W. (1995). "Island arc response to shallow subduction of the Cocos Ridge, Costa Rica," in *Geologic and Tectonic Development of the Caribbean Plate Boundary in Southern Central America*, , Vol. 295, ed. P. Mann (Boulder, CO: Geological Society of America), 235–262.

Kopp, H., Flueh, E. R., Papenberg, C., and Klaeschen, D. (2004). Seismic investigations of the O'Higgins seamount group and Juan Fernandez Ridge: aseismic ridge emplacement and lithosphere hydration. *Tectonics* 23:TC2009. doi: 10.1029/2003TC001590

Krabbenhoeft, A., Bialas, J., Kopp, H., Kukowski, N., and Hübscher, C. (2004). Crustal structure of the Peruvian continental margin from wide-angle seismic studies. *Geophys. J. Intern.* 159, 749–764. doi: 10.1111/j.1365-246x.2004.02425.x

Kukowski, N., Hampel, A., Hoth, S., and Bialas, J. (2008). Morphotectonic and morphometric analysis of the Nazca plate and the adjacent offshore Peruvian continental slope – Implications for submarine landscape evolution. *Mar. Geol.* 254, 107–120. doi: 10.1016/j.margeo.2008.05.017

Kumar, A., Wagner, L. S., Beck, S. L., Long, M. D., Zandt, G., Young, B., et al. (2016). Seismicity and state of stress in the central and southern Peruvian flat slab. *Earth Planet. Sci. Lett.* 441, 71–80. doi: 10.1016/j.epsl.2016.02.023

Lefeldt, M., Ranero, C. R., and Grevemeyer, I. (2012). Seismic evidence of tectonic control on the depth of water influx into incoming oceanic plates at subduction trenches. *Geochem. Geophys. Geosys.* 13:Q05013. doi: 10.1029/2012GC004043

Lim, H., Kim, Y., Clayton, R. W., and Thurber, C. H. (2018). Seismicity and structure of Nazca Plate subduction zone in southern Peru. *Earth Planet. Sci. Lett.* 498, 334–347. doi: 10.1016/j.epsl.2018.07.014

Lonsdale, P. (2005). Creation of the cocos and nazca plates by fission of the farallon plate. *Tectonophysics* 404, 237–264. doi: 10.1016/j.tecto.2005.05.011

MacMillan, I., Gans, P. B., and Alvarado, G. (2004). Middle Miocene to present plate tectonic history of the southern central american volcanic arc. *Tectonophysics* 404, 237–264.

Marcaillou, B., Collot, J.-Y., Ribodetti, A., d'Acremont, E., Mahamat, A.-A., and Alvarado, A. (2016). Seamount subduction at the North-Ecuadorian convergent margin: effects on structures, inter-seismic coupling and seismogenesis. *Earth Planet. Sci. Lett.* 433, 146–158. doi: 10.1016/j.epsl.2015.10.043

Marot, M., Monfret, T., Pardo, M., Ranalli, G., and Nolet, G. (2013). A double seismic zone in the subducting Juan Fernandez Ridge of the Nazca Plate (32° S), central Chile. *J. Geophys Res.* 118, 3462–3475. doi: 10.1002/jgrb.50240

Meade, C., and Jeanloz, R. (1991). Deep-focus earthquakes and recycling of water into the Earth's mantle. *Science* 252, 68–72. doi: 10.1126/science.252.5002.68

Michaud, F., Witt, C., and Royer, J.-Y. (2009). "Influence of the subduction of the Carnegie volcanic ridge on Ecuadorian geology: reality and fiction," in *Backbone of the Americas: Shallow Subduction, Plateau Uplift, and Ridge and Terrane Collision*, Vol. 204, eds S. M. Kay, V. A. Ramos, and W. R. Dickinson (Washington, DC: Geological Society of America Memoir). doi: 10.1130/2009.1204

Morell, K. D., Kirby, E., Fischer, D. M., and van Soest, M. (2012). Geomorphic and exhumational response of the Central American Volcanic arc to Cocos Ridge subduction. *J. Geophys. Res.* 117:4409. doi: 10.1029/2011JB008969

Moscoso, E., and Grevemeyer, I. (2015). Bending-related faulting of the incoming oceanic plate and its effect on lithospheric hydration and seismicity: a passive an active seismological study offshore Maule, Chile. *J. Geodyn.* 90, 58–70. doi: 10.1016/j.jog.2015.06.007

Mueller, R. D., Sdrolias, M., Gaina, C., and Roest, W. R. (2008). Age, spreading rates, and spreading asymmetry of the world's ocean crust. *Geochem. Geophys. Geosys.* 9:Q04006. doi: 10.1029/2007GC001743

Ohuchi, T., Lei, X., Ohfuji, H., Higo, Y., Tange, Y., Sakai, T., et al. (2017). Intermediate-depth earthquakes linked to localized heating in dunite and harzburgite. *Nat. Geosci.* 10, 771–776. doi: 10.1038/ngeo3011

Okazaki, K., and Hirth, G. (2016). Dehydration of lawsonite could directly trigger earthquakes in subducting oceanic crust. *Nature* 530, 81–84. doi: 10.1038/nature16501

Padrón-Navarta, J. A., Sánchez-Vizcaíno, V. L., Hermann, J., Connolly, J. A. D., Garrido, C. J., Gómez-Pugnaire, M. T., et al. (2013). Tschermak's substitution in antigorite and consequences for phase relations and water liberation in high-grade serpentinites. *Lithos* 178, 186–196. doi: 10.1016/j.lithos.2013.02.001

Peacock, S. M. (2001). Are the lower planes of double seismic zones caused by serpentine dehydration in subducting oceanic mantle? *Geology* 29, 299–302.

Peacock, S. M., van Keken, P. E., Holloway, S. D., Hacker, B. R., Abers, G. A., and Fergason, R. L. (2005). Thermal structure of the Costa Rica–Nicaragua subduction zone. *Phys. Earth Planet. Inter.* 149, 187–200. doi: 10.1016/j.pepi.2004.08.030

PeruSE (2013). *Peru Subduction Experiment*. Pasadena: Caltech.

Pilger, R. H. (1981). Plate reconstructions, aseismic ridges, and low-angle subduction beneath the Andes. *Geol. Soc. Am. Bull.* 29, 448–456.

Plümper, O., Botan, A., Los, C., Liu, Y., Malthe-Sørenssen, A., and Jamtveit, B. (2017). Fluid-driven metamorphism of the continental crust governed by nanoscale fluid flow. *Nat. Geosci.* 10, 685–690. doi: 10.1038/ngeo3009

Poli, P., Prieto, G., Rivera, E., and Ruiz, S. (2016). Earthquakes initiation and thermal shear instability in the Hindu Kush intermediate depth nest. *Geophys. Res. Lett.* 43, 1537–1542. doi: 10.1002/2015gl067529

Prieto, G. A., Florez, M., Barrett, S. A., Beroza, G. C., Pedraza, P., Blanco, J. F., et al. (2013). Seismic evidence for thermal runaway during intermediate-depth earthquake rupture. *Geophys. Res. Lett.* 40, 6064–6068. doi: 10.1002/2013gl058109

Proctor, B., and Hirth, G. (2015). Role of pore fluid pressure on transient strength changes and fabric development during serpentine dehydration at mantle conditions: implications for subduction-zone seismicity. *Earth Planet. Sci. Lett.* 421, 1–12. doi: 10.1016/j.epsl.2015.03.040

Proctor, B., and Hirth, G. (2016). Ductile to brittle" transition in thermally stable antigorite gouge at mantle pressures. *J. Geophys. Res. Solid Earth* 121, 1652–1663. doi: 10.1002/2015jb012710

Protti, M., Guendel, F., and McNally, K. (1994). The geometry of the Wadati-Benioff zone under southern Central America and its tectonic significance: results from a high-resolution local seismographic network. *Phys. Earth Planet. Int.* 84, 271–287. doi: 10.1016/0031-9201(94)90046-9

Raleigh, C. B., and Paterson, M. S. (1965). Experimental deformation of serpentinite and its tectonic implications. *J. Geophys. Res.* 70, 3965–3985. doi: 10.1029/jz070i016p03965

Ranero, C. R., Phipps Morgan, J., McIntosh, K., and Reichert, C. (2003). Bending-related faulting and mantle serpentinization at the Middle America trench. *Nature* 425, 367–373. doi: 10.1038/nature01961

Ranero, C. R., Villaseñor, A., Morgan, J. P., and Weinrebe, W. (2005). Relationship between bend-faulting at trenches and intermediate-depth seismicity. *Geochem. Geophys. Geosys.* 6:Q12002. doi: 10.1029/2005GC000997

Ringwood, A. E. (1982). Phase transformations and differentiation in subducted lithosphere: implications for mantle dynamics, basalt petrogenesis, and crustal evolution. *J. Geol.* 90, 611–643. doi: 10.1086/628721

Robinson, A. H., Peirce, C., and Funnell, M. J. (2018). Construction and subduction of the Louisville Ridge, SW Pacific – insights from wide-angle seismic data modelling. *Geophys. J. Int.* 214, 2222–2245. doi: 10.1093/gji/ggy397

Rosenbaum, G., Giles, D., Saxon, M., Betts, P. G., Weinberg, R. F., and Duboz, C. (2005). Subduction of the Nazca Ridge and the Inca Plateau: insights into the formation of ore deposits in Peru. *Earth Planet. Sci. Lett.* 239, 18–32. doi: 10.1016/j.epsl.2005.08.003

Rosenbaum, G., Sandiford, M., Caulfield, J., and Garrison, J. M. (2018). A trapdoor mechanism for slab tearing and melt generation in the northern Andes. *Geology* 47, 23–26. doi: 10.1130/g45429.1

Sallares, V., Charvis, P., Flueh, E., and Bialas, J. (2003). Seismic structure of Cocos and Mapelo volcanic ridges and implications for hot spot – ridge interaction. *J. Geophys. Res.* 108:2431. doi: 10.1029/2003JB002431

Sallares, V., Charvis, P., Flueh, E., and Bialas, J. (2005). Seismic structure of the Carnegie ridge and the nature of the Galapagos hotspot. *Geophys. J. Int.* 161, 763–788. doi: 10.1111/j.1365-246x.2005.02592.x

Sandiford, D., Moresi, L., Sandiford, M., and Yang, T. (2019). Geometric controls on flat slab seismicity. *Earth Planet. Sci. Lett.* 527:115787. doi: 10.1016/j.epsl.2019.115787

Scholtz, C. H., and Small, C. (1997). The effect of seamount subduction on seismic coupling. *Geology* 25, 487–490.

Scire, A., Zandt, G., Beck, S., Long, M., Wagner, L., Minaya, E., et al. (2015). Imaging the transition from flat to normal subduction: variations in the structure of the Nazca slab and upper mantle under southern Peru and northwestern Bolivia. *Geophys. J. Int.* 204, 457–479. doi: 10.1093/gji/ggv452

Shillington, D. J., Bécel, A., Nedimoviæ, M. R., Kuehn, H., Webb, S. C., Abers, G. A., et al. (2015). Link between plate fabric, hydration and subduction zone seismicity in Alaska. *Nat. Geosci.* 8, 961–964. doi: 10.1038/ngeo2586

Staudigel, H., Hart, S. R., Schmincke, H.-U., and Smith, B. M. (1989). Cretaceous ocean crust at DSDP Sites 417 and 418: carbon uptake from weathering versus loss by magmatic outgassing. *Geochim. Cosmochim. Acta* 53, 3091–3094. doi: 10.1016/0016-7037(89)90189-0

Staudigel, H., Plank, T., White, B., and Schmincke, H.-U. (1996). "Geochemical fluxes during seafloor alteration of the basaltic upper oceanic crust: DSDP Sites 417 and 418," in *Subduction: Top to Bottom*, ed. E. Bebout (Washington, DC: American Geophyiscal Union), 19–38. doi: 10.1029/gm096p0019

van Hunen, J., van den Berg, A. P., and Vlaar, N. J. (2002). On the role of subducting oceanic plateaus in the development of shallow flat subduction. *Tectonophysics* 352, 317–333. doi: 10.1016/s0040-1951(02)00263-9

von Huene, R., Corvalan, J., Flueh, E. R., Hinz, K., Korstgard, J., Ranero, C. R., et al. (1997). Tectonic control of the subducting juan fernandez ridge on the andean margin near Valparaiso. *Chile. Tecton.* 16, 474–488. doi: 10.1029/96tc03703

von Huene, R., Ranero, C. R., Weinrebe, W., and Hinz, K. (2000). Quaternary convergent margin tectonics of Costa Rica, segmentation of the Cocos Plate, and Central American volcanism. *Tectonics* 19, 314–334. doi: 10.1029/1999tc001143

Wagner, L. S., Beck, S. L., and Long, M. D. (2010). *PerU Lithosphere and Slab Experiment. International Federation of Digital Seismograph Networks. Dataset/Seismic Network*. doi: 10.7914/SN/ZD_2010

Wagner, L. S., and Okal, E. A. (2019). The Pucallpa nest and its constraints on the geometry of the Peruvian Flat Slab. *Tectonophysics* 762, 97–108. doi: 10.1016/j.tecto.2019.04.021

Walther, C. H. E. (2003). The crustal structure of the Cocos Ridge off Costa Rica. *J. Geophys. Res.* 108:888. doi: 10.1029/2001JB000888

Watts, A. B., Weissel, J. K., Duncan, R. A., and Larson, R. L. (1988). Origin of the Louisville Ridge and its relationship to the Eltanin fracture zone system. *J. Geophys. Res.* 93, 3051–3077.

Woods, M. T., and Okal, E. A. (1994). The structure of the Nazca ridge and Sala y Gomez seamount chain from the dispersion of Rayleigh waves. *Geophys. J. Int.* 117, 205–222. doi: 10.1111/j.1365-246x.1994.tb03313.x

Yamasaki, T., and Seno, T. (2003). Double seismic zone and dehydration embrittlement of the subducting slab. *J. Geophys. Res.* 108:2212. doi: 10.1029/2002JB001918

Yañez, G. A., Cembrano, J., Pardo, M., Ranero, C. R., and Selles, D. (2002). The challenger – Juan Fernandez – Maipo major tectonic transition of the Nazca – Andean subduction system at 33 – 34 S: geodynamic evidence and implications. *J. South Am. Earth Sci.* 15, 23–38. doi: 10.1016/s0895-9811(02)00004-4

Yañez, G. A., Ranero, C. R., von Huene, R., and Diaz, J. (2001). Magnetic anomaly interpretation across the southern central Andes (32 – 34 S): the role of the Juan Fernandez Ridge in the late Tertiary evolution of the margin. *J. Geophys Res.* 106, 6325–6345. doi: 10.1029/2000jb900337

Yepes, H., Audin, L., Alvarado, A., Beauval, C., Aguilar, J., Font, Y., et al. (2016). A new view for the geodynamics of Ecuador: implication in seismogenic source definition and seismic hazard assessment. *Tectonics* 35, 1249–1279. doi: 10.1002/2015tc003941

Zhan, Z. (2017). Gutenberg–Richter law for deep earthquakes revisited: a dual-mechanism hypothesis. *Earth Planet. Sci. Lett.* 461:30. doi: 10.1016/j.epsl.2016.12.030

Conflict of Interest: The authors declare that the research was conducted in the absence of any commercial or financial relationships that could be construed as a potential conflict of interest.